



HAL
open science

Probing the effects of redox conditions and dissolved Fe²⁺ on nanomagnetite stoichiometry by wet chemistry, XRD, XAS and XMCD

Phoomipat Jungcharoen, Mathieu Pédrot, Fadi Choueikani, Mathieu Pasturel, Khalil Hanna, Frank Heberling, Marawit Tesfa, Remi Marsac

► To cite this version:

Phoomipat Jungcharoen, Mathieu Pédrot, Fadi Choueikani, Mathieu Pasturel, Khalil Hanna, et al.. Probing the effects of redox conditions and dissolved Fe²⁺ on nanomagnetite stoichiometry by wet chemistry, XRD, XAS and XMCD. *Environmental science.Nano*, 2021, 8 (8), pp.2098-2107. 10.1039/D1EN00219H . insu-03263142

HAL Id: insu-03263142

<https://insu.hal.science/insu-03263142>

Submitted on 17 Jun 2021

HAL is a multi-disciplinary open access archive for the deposit and dissemination of scientific research documents, whether they are published or not. The documents may come from teaching and research institutions in France or abroad, or from public or private research centers.

L'archive ouverte pluridisciplinaire **HAL**, est destinée au dépôt et à la diffusion de documents scientifiques de niveau recherche, publiés ou non, émanant des établissements d'enseignement et de recherche français ou étrangers, des laboratoires publics ou privés.

Environmental Science Nano

Accepted Manuscript

This article can be cited before page numbers have been issued, to do this please use: P. Jungcharoen, M. Pédrot, F. Choueikani, M. Pasturel, K. Hanna, F. Heberling, M. Tesfa and R. Marsac, *Environ. Sci.: Nano*, 2021, DOI: 10.1039/D1EN00219H.



This is an Accepted Manuscript, which has been through the Royal Society of Chemistry peer review process and has been accepted for publication.

Accepted Manuscripts are published online shortly after acceptance, before technical editing, formatting and proof reading. Using this free service, authors can make their results available to the community, in citable form, before we publish the edited article. We will replace this Accepted Manuscript with the edited and formatted Advance Article as soon as it is available.

You can find more information about Accepted Manuscripts in the [Information for Authors](#).

Please note that technical editing may introduce minor changes to the text and/or graphics, which may alter content. The journal's standard [Terms & Conditions](#) and the [Ethical guidelines](#) still apply. In no event shall the Royal Society of Chemistry be held responsible for any errors or omissions in this Accepted Manuscript or any consequences arising from the use of any information it contains.

Probing the effects of redox conditions and dissolved Fe²⁺ on nanomagnetite stoichiometry by wet chemistry, XRD, XAS and XMCD

Phoomipat Jungcharoen¹, Mathieu Pédrot¹, Fadi Choueikani², Mathieu Pasturel³, Khalil Hanna⁴,
Frank Heberling⁵, Marawit Tesfa¹, Rémi Marsac^{1*}

¹ Univ Rennes, CNRS, Géosciences Rennes – UMR 6118, F-35000 Rennes, France.

E-mail: remi.marsac@univ-rennes1.fr

² Synchrotron SOLEIL, L'ormes des Merisiers, Saint Aubin BP48, 91192 Gif sur Yvette cedex, France.

³ Univ Rennes, CNRS, ISCR – UMR 6226, F-35000, Rennes, France

⁴ Univ Rennes, Ecole Nationale Supérieure de Chimie de Rennes, CNRS, ISCR-UMR 6226, F-35000, Rennes, France.

⁵ Institut für Nukleare Entsorgung, Karlsruhe Institute of Technology, P.O. Box 3640, D-76021 Karlsruhe, Germany

Keywords: magnetite, maghemite, nanoparticle, oxidation, recharge, spin canting, XAS, XMCD.

Abstract

Magnetite nanoparticles, commonly found in subsurface environments, are extensively used in various applications such as environmental remediation, catalysis, electronics and medicine. However, the oxidative transformation of magnetite (mixed-valent Fe-oxide) into maghemite (Fe(III)-oxide) that drastically affects magnetic, catalytic and redox properties of the mineral, is still poorly understood. In the present study, a thorough characterization of both particle core and surface of magnetite was performed to accurately assess the relationship between mineral composition and reactivity within the magnetite/maghemite core-shell structure. Previous work showed that X-ray absorption spectra (XAS) and X-ray magnetic circular dichroism (XMCD) can provide key insights into magnetite stoichiometry ($R = \text{Fe(II)}/\text{Fe(III)}$) of 10 nm sized particles, as compared to wet chemistry and X-ray diffraction (XRD). In the present study, XMCD signals have been used to further characterize the complex reactions involved in the magnetite/maghemite system upon oxidation and recharge processes, *e.g.* decreasing R from 0.5 to 0.1 using H_2O_2 or increasing from 0.1 to 0.5 through dissolved Fe^{2+} amendment. Indeed, surface recrystallization processes, induced by oxidation as well as Fe^{2+} diffusion into the solid phase and/or redistribution of electron equivalents between the aqueous solution and the magnetite bulk, led to decreased spin canting effects, altering XMCD signals. This study provides a fundamental understanding of the processes occurring in the magnetite/maghemite system upon the alteration of the redox conditions and offers a more accurate method for the determination of magnetite stoichiometry by XMCD.

Environmental significance

Nanometric magnetite is a ubiquitous mixed Fe(II)-Fe(III) oxide in soils and sediments. This reactive nanosized mineral plays a key role in the biogeochemical cycling of trace elements and affects the mobility, redox transformation, and toxicity of various organic and inorganic pollutants. The stoichiometry (Fe(II)/Fe(III)) of magnetite nanoparticles, a key parameter controlling their reactivity, is subjected to large variations especially in Fe-rich subsurface environments experiencing alternating anoxic and oxic periods. Unlike more classical techniques, X-ray magnetic circular dichroism spectroscopy was found here to be a powerful tool to uncover surface recrystallization processes throughout oxidation-recharge cycles of magnetite nanoparticles or their amendment with an excess of Fe²⁺. This work sheds light on an overlooked process occurring at the nanomagnetite-water interface, which enriches our understanding of the behavior and reactivity of mixed-valence oxides in environmental settings.

1. Introduction

Magnetite nanoparticles have recently aroused great interest due to their large reactive surface area, good inherent magnetism, and redox properties¹. They have been evaluated as promising materials in various fields including, for instance, cancer diagnosis² and therapy^{3,4}, energy storage^{5,6}, catalysis science⁷, and water treatment^{8,9}. Furthermore, magnetite (Fe₃O₄) is a corrosion product of elemental iron and has recently been shown to control the surface properties and reactivity of nanosized zero-valent iron used for soil and groundwater remediation¹⁰. Magnetite is ubiquitous in the earth's crust, soils, and sediments and exists under various particle sizes, morphologies, and stoichiometries^{11–13}. It also plays an important role as electron source or sink for microorganisms.¹⁴ The stoichiometry of the particles (R) is one of the most important factors in controlling the reactivity of magnetite, *e.g.* (i) reduction kinetics of nitroaromatic compounds^{15,16}, (ii) adsorption capacity of organic compounds¹⁷, and (iii) sorption and redox speciation of inorganic contaminants¹⁸. R can be defined as follows:

$$R = \text{Fe(II)/Fe(III)} \quad (1)$$

R equals 0.5 for a perfectly stoichiometric (Fe₃O₄) magnetite and 0 for maghemite (γ-Fe₂O₃), the fully oxidized form of magnetite, whose chemical formula can also be written Fe_{8/3}O₄ by analogy with that of magnetite. Partial oxidation of magnetite can lead to the formation of non-stoichiometric magnetite (Fe_{3-δ}O₄) with 0 ≤ R ≤ 0.5 (0 ≤ δ ≤ 1/3). If non-stoichiometric magnetite is exposed to a source of dissolved Fe(II), perfectly stoichiometric magnetite (*i.e.* R = 0.5) can be restored through oxidation of a Fe(II) ion adsorbed at the surface and reduction of underlying octahedral Fe(III) in the magnetite structure, as previously demonstrated using bulk characterization techniques such as Mössbauer spectroscopy, X-ray diffraction (XRD) or wet chemistry¹⁵.

Heterogeneous redox reactions may occur at the magnetite-water interface with the potential formation of magnetite-maghemite core-shell structures¹⁹. The surface properties of magnetite can be altered upon Fe(II)-recharge. Indeed, complex surface reactions can take place when stoichiometric magnetite is equilibrated with dissolved Fe(II), such as rapid atomic exchange²⁰, redistribution of electron equivalents between bulk and the outermost surface of particles²¹, and surface-mediated electron transfer with redox-sensitive species in solution²². It is, therefore, necessary to thoroughly characterize both the bulk and surface of magnetite to accurately

1
2
3 evaluate the surface reactivity changes through oxidation-recharge processes, which cannot be
4 done by Mossbauer, XRD or wet chemistry. Thanks to their chemical selectivity and valence
5 state sensitivity, X-ray absorption spectroscopy (XAS) and X-ray magnetic circular dichroism
6 (XMCD) are unique tools to separately probe the electronic properties of the $3d$ transition
7 element Fe. The total electron yield (TEY) used as detection mode is sensitive to the surface of
8 the (nano)particles ($\sim 4\text{-}5\text{ nm}$)²³. Isotropic XAS, i.e. obtained in the absence of a magnetic field,
9 can be used to probe the Fe(II)/Fe(III) ratio of Fe-oxides but is not specific to spinel structures
10 like magnetite. By contrast, XMCD enables to distinguish the tetrahedral (T_d) and octahedral
11 (O_h) iron and their oxidation state in magnetic compounds. XMCD spectra of magnetite typically
12 show two negative peaks due to Fe(II) and Fe(III) on a O_h site, and a positive one due to Fe(III)
13 on a T_d site, whose relative intensities allow determining the magnetite stoichiometry. For these
14 reasons, XAS and XMCD at the Fe $L_{2,3}$ -edges were used in several studies to elucidate the
15 structure and properties of magnetite surfaces^{21,24-31}.

16
17 The XMCD signal of nanostructured magnetically ordered materials is also sensitive to spin
18 canting^{29,32-34}, which results from structural disorder, either in the interior or at the surface,
19 giving rise to the misalignment of atomic magnetic moments. The spin canting effect is
20 visualized in XMCD spectra through the decrease in the intensity of the peaks of Fe(II) _{O_h} and
21 Fe(III) _{O_h} relative to that of Fe(III) _{T_d} .^{29,32-34} The fact that the XMCD signal is not only sensitive
22 to the Fe oxidation state but also to spin canting may hamper the determination of magnetite
23 surface stoichiometry. Because spin canting globally minors the signal of Fe(II) relative to that
24 of Fe(III), its effect might be wrongly attributed to partial oxidation of magnetite. Conversely, in
25 a recent study,²¹ the Fe(II) signal of a stoichiometric magnetite in aqueous suspension was shown
26 to increase upon addition of dissolved Fe²⁺, which suggested the formation of
27 hyperstoichiometric or “cation-excess” magnetite. However, because recrystallization processes
28 can decrease spin canting at the magnetite surface,^{29,33} an alternative interpretation to the
29 formation of hyperstoichiometric magnetite²¹ might be the decrease in spin canting effect upon
30 Fe²⁺-induced recrystallization at the magnetite surface. Therefore, the latter hypothesis deserves
31 further investigation.

32
33 The aim of this study is to assess the oxidation and recharge processes of nanosized magnetite
34 ($\sim 10\text{ nm}$), using H₂O₂ and dissolved Fe(II), respectively, as well as the impact of the presence of
35
36
37
38
39
40
41
42
43
44
45
46
47
48
49
50
51
52

1
2
3 a dissolved Fe(II) excess on the magnetite surface and bulk structure using a combination of
4 techniques: wet chemistry, XRD, XAS, and XMCD. In particular, the impacts of recrystallization
5 processes induced by H₂O₂ oxidation or Fe(II) amendment on spin canting were carefully
6 addressed to determine the Fe(II)/Fe(III) ratio from XMCD data. This study provides a
7 comprehensive understanding of the behavior and reactivity of magnetite nanoparticles and paves
8 the way for developing more accurate methods to determine magnetite stoichiometry in aqueous
9 solution. As a result, these findings will have strong implications in various research fields
10 including medicine, catalysis, electrochemistry, and environmental research and applications.

2. Materials and methods

2.1 Materials

All chemicals were of analytical grade or better and were purchased from Sigma-Aldrich. The sample solutions were prepared with ultrapure “MilliQ” water (specific resistivity 18.2 MΩ cm). All experiments were carried out in an anaerobic chamber (N₂-glovebox, JACOMEX, O_{2(g)} < 1 ppm), and all solutions were purged with N_{2(g)} for at least 12 h inside the glovebox before use.

2.2 Synthesis of magnetites with various stoichiometries

Stoichiometric magnetite (R0.5) has been synthesized in an N₂-glovebox following a well-known room temperature aqueous precipitation method, which produces ~10 nm particles^{35,36}. A 0.5 M HCl solution (40 mL) containing a 0.5 M FeCl₂ and 1 M FeCl₃ (1:2 molar ratio) was added dropwise into a 0.5 M NaOH solution (250 mL) while continuously stirring, leading to instantaneous precipitation of magnetite particles. After the synthesis, the solid phase was washed three times with ultrapure water, pH 8.5 (adjusted using NaOH) to avoid the release of Fe²⁺, as observed in previous work^{17,37}, and thus, to guarantee a stoichiometry of R0.5. Specific stoichiometric amounts of H₂O₂ were added to R0.5 to produce different sets of partly oxidized non-stoichiometric magnetites (R0.1, R0.2, R0.3, R0.4)^{17,38}. The non-stoichiometric magnetites were washed with ultrapure water (at pH = 8.5) to remove residual H₂O₂.

Effective Fe(II)/Fe(III) ratios (R_{eff}) of all magnetites (R0.1, R0.2, R0.3, R0.4, and R0.5) were determined by acid digestion of magnetites in 0.6 M HCl during 3 days, followed by spectrophotometric determination of dissolved [Fe(II)] and total [Fe] (= [Fe(III)] + [Fe(II)]) using

the 1-10 phenanthroline colorimetric method³⁹. Results were in excellent agreement with values expected from the amount of added H₂O₂, as in previous studies^{15,17,38}. Repetition of acid digestion followed by spectrophotometry led to an error of ±0.01 on the determination of R_{eff}.

2.3 Batch studies

All magnetite aqueous suspensions were prepared for a total Fe concentration of 6.5 mM (~0.5 g L⁻¹ of magnetite) in 10 mM NaCl solutions, in 15 mL polypropylene tubes containing 10 mL of solution. HCl and NaOH were used to adjust pH to a final value of 8.5 (no buffer was used). The impact of dissolved Fe(II) addition on the recharge of R0.1 to R0.2, R0.3, R0.4 or R0.5 was investigated by adding small amounts of a 100 mM FeCl₂ solution. The impact of the presence of an excess of Fe(II) on R0.5 was investigated by adding 250, 500, 1000, and 2500 μM Fe²⁺ to R0.5. Although magnetite interaction with Fe²⁺ proceeds within less than one day at pH > 7^{15,17}, a reaction time of 20 days was applied to ensure chemical equilibrium. pH was controlled and adjusted regularly if needed. After 20 days, a fraction of the solid phase was separated from the solution using a magnet to determine R_{eff} by acid digestion followed by spectrophotometry. An aliquot of the suspension was filtered using 0.2 μm cellulose acetate filters (Sartorius Minisart). The absence of Fe nanoparticles in the filtrate was checked by dynamic light scattering (VASCO Flex). Dissolved [Fe(II)] was measured by spectrophotometry (dissolved Fe(III) was never detected). Knowing the total [Fe(II)] and [Fe(III)] in the initial suspension (*i.e.* solid and solution) and dissolved [Fe(II)]_{aq} after filtration, R_{eff} could be calculated according to the following equation:

$$R_{\text{eff}} = ([\text{Fe(II)}]_{\text{Total}} - [\text{Fe(II)}]_{\text{aq}}) / ([\text{Fe(III)}]_{\text{Total}}) \quad (2)$$

R_{eff} determined by acid digestion or by measurement of [Fe(II)]_{aq} using eq. 2 were in excellent agreement.

All syntheses were carried out at Geosciences Rennes. A fraction of samples was transported to the SOLEIL Synchrotron facility at the DEIMOS⁴⁰ beamline in 1 mL tubes, placed in airtight bottles that had been closed in the N₂-glovebox. At SOLEIL, samples were handled in an Ar-glovebox connected to the end station of DEIMOS. To ensure that no sample oxidation occurred

1
2
3 during transport, the samples were brought back to Geosciences Rennes after analysis at the
4 DEIMOS beamline, and the Fe(II)/Fe(III) ratio of the suspension was checked by acid digestion.

2.4 Characterization

5
6
7
8
9
10
11
12
13
14
15
16
17
18
19
20
21
22
23
24
25
26
27
28
29
30
31
32
33
34
35
36
37
38
39
40
41
42
43
44
45
46
47
48
49
50
51
52
53
54
55
56
57
58
59
60
TEM and XRD. Transmission electron microscopy (TEM; Jeol JEM 1230 microscope) was used for magnetite nanoparticles characterization. A small aliquot of magnetite suspension was diluted with ultrapure water (at pH = 8.5) and sonicated for 20 min. A droplet of the diluted suspension was deposited on a carbon-coated 200 mesh copper grid and dried inside the anaerobic chamber. Samples were transported to the microscope under an N₂ atmosphere using a hermetic holder and the samples were analyzed at an acceleration voltage of 200 kV. Average particle diameters were determined by measuring 100 particles.

Powder X-ray diffraction (XRD) was performed on a Bruker D8 Advance diffractometer working with a monochromatized Cu K_{α1} radiation ($\lambda = 1.5406 \text{ \AA}$) and equipped with a LynxEye fast detector enabling a photon energy selection and thus the removal of Fe-fluorescence background signal. Magnetite suspension was placed on a misoriented Si single crystal holder and dried for 2 h in an anaerobic chamber. To avoid the oxidation of magnetite during the XRD analysis, the dried samples were covered by a drop of glycerol. The samples were scanned in the 2θ range from 20° to 120° with steps of 0.02° and an integration time of 716 s per step. Rietveld refinement of the XRD patterns, using the FullProf software⁴¹, enabled to determine (i) the cell parameters of the phase and (ii) the average crystallite size by fitting the Lorentzian broadening of the peaks compared to a standard corundum sample and deconvoluting the instrumental contribution from the total FWHM using a Thompson-Cox-Hastings profile function⁴².

XAS and XMCD signals were recorded at the Fe $L_{2,3}$ edges (700 – 730 eV) on the DEIMOS beamline at the synchrotron light source SOLEIL⁴⁰. The measurement protocol was detailed in previous studies^{44,45}. Colloidal suspensions of nanoparticles were drop-casted on silicon substrates and dried at room temperature, in the Ar-glove box (O_{2(g)} < 1 ppm) connected to the end station. The silicon substrates were fixed on a sample holder and transferred into the cryomagnet, under ultra-high vacuum (UHV-10⁻¹⁰ mbar). All spectra were measured in Total Electron Yield mode (TEY) at 4.2 K under UHV conditions and an applied magnetic field H (H⁺ = +6 Tesla and H⁻ = -6 Tesla). The beam size was 800*800 μm² and the resolution was 100 meV. XAS and XMCD spectra were plotted by considering the absorption cross-section measured with left (σ_L) and right (σ_R) circularly polarized X-rays. Isotropic XAS were plotted as $\sigma_{XAS} = (\sigma_+ + \sigma_-)/2$ and XMCD

spectra were plotted as $\sigma_{\text{XMCD}} = (\sigma_+ - \sigma_-)$ where $\sigma_+ = [\sigma_{\text{L}}(\text{H}^+) + \sigma_{\text{R}}(\text{H}^+)]/2$ and $\sigma_- = [\sigma_{\text{L}}(\text{H}^-) + \sigma_{\text{R}}(\text{H}^-)]/2$. The circularly polarized X-rays are provided by an Apple-II HU-52 helical undulator for both XAS and XMCD measurements and by sweeping the magnetic field from +6T to -6T. Both isotropic XAS and XMCD signals were normalized by dividing the raw signal by the edge jump of the isotropic XAS.

3. Results and discussion

3.1 Effects of oxidation on magnetite characteristics

The individual sizes and shapes of magnetite nanoparticles were measured by TEM imaging (Figure S1). The synthesized magnetite and oxidation products displayed nearly spherical shapes and similar sizes with diameters of ca. 10 nm (i.e. between 8.9 ± 2.1 and 11.5 ± 1.5 nm; Table S1). This agrees with previous work³⁶ where the oxidation of iron nanoparticles (magnetite to maghemite) did not significantly affect the magnetite particle size. The XRD patterns of magnetite nanoparticles have previously been shown to depend on the stoichiometry of the nanoparticles³⁸. Cell parameters of stoichiometric magnetite range from 8.39 to 8.40 Å^{11,46}. XRD analysis confirmed the purity of R0.5 (8.3976 Å; Table S1 and Figure. S2). Oxidation of R0.5 leads to non-stoichiometric magnetite with smaller cell parameters (e.g. 8.3685 Å for R0.1; Table S1 and Figure. S2)^{11,30,38,47}. Cell parameters of these samples fall between that of magnetite and maghemite (8.34 Å)¹¹ which confirms that these samples are magnetite-maghemite solid-solutions. It is interesting to note that R does not seem to evolve linearly with the cell parameter in the present work, by contrast with Gorki et al.'s findings³⁸ but in agreement with Pearce et al.³⁰ (Figure S3). However, given the small discrepancies between all these studies, results might be considered in relatively good agreement.^{30,38} Bragg peaks enlargement observed on XRD patterns (Figure S2) was treated during Rietveld refinements as “crystallite size” effect. This led to ca. 6.3-9.4 nm crystallites, in relatively good agreement with TEM when keeping in mind that differentiating between size effect, crystallographic defects or internal strains by XRD is difficult for nanoparticles⁴⁸.

Figure 1a shows the isotropic XAS spectra at $L_{2,3}$ edges of stoichiometric nanomagnetite (R0.5) and oxidation products (R0.1 to R0.4) at pH 8. They are typical spectra of ferrite spinel structures^{21,24-29}. The Fe L_3 -edge show two main contributions at 706.9 eV (I_1) and 707.2 eV (I_2) that correspond to Fe(II) on O_h sites (I_1), and Fe(III) on O_h and T_d sites at 707.2 eV (I_2),

1
2
3
4
5
6
7
8
9
10
11
12
13
14
15
16
17
18
19
20
21
22
23
24
25
26
27
28
29
30
31
32
33
34
35
36
37
38
39
40
41
42
43
44
45
46
47
48
49
50
51
52
53
54
55
56
57
58
59
60

respectively. The evolution of the I_1/I_2 ratio versus the R provides information about the amount of Fe(II) at the surface of the nanoparticles. In addition, the series of pre-edge-peaks between 703 and 705 eV, increased with increasing R, which is attributed to the increase in the amount of Fe(II) in the near-surface region of the nanoparticles from R0.1 to R0.5. Corresponding XMCD spectra, illustrated in Figure 1b, present three main peaks at the L_3 edge. The peak S_1 corresponds to both Fe(II) and Fe(III) on O_h sites, but is dominated by Fe(II), the peak S_2 corresponds to the contribution of Fe(III) in T_d sites while the peak S_3 is attributed to Fe(III) on O_h sites. S_1 and S_3 are coupled antiparallel to S_2 due to the ferromagnetic behavior of the inverse spinel structure of $Fe_{3-\delta}O_4$ nanoparticles. A very low intensity of S_1 (R0.1) with an oscillation between S_1 and S_2 corresponds to an iron oxide spinel structure with deficiency in Fe(II) atoms, that is, a structure very close to maghemite^{27,28,49}. However, the XMCD of R0.1 also shows characteristic features of magnetite such as pre-peaks between 703 and 705 eV, which confirms the presence of Fe(II) in the structure.²⁸ The increase of S_1 versus R indicates the increase of the amount Fe(II) in the structure.

The decrease in S_1 intensity with constant S_3 intensity explains the decreasing Fe(II) content from R0.4 to R0.1. However, the intensities of both negative peaks S_1 and S_3 are smaller for R0.5 than for R0.4 (inset to Figure 1). This is consistent with previous investigations, which have ascribed this phenomenon to surface spin canting effects with increased spin disorder occurring preferentially at the octahedral sites^{29,33}. The growth process of maghemite is mediated by Fe^{2+} cations and vacancy diffusion that can give rise to structural reorganization and a lower degree of structural disorder. This mechanism could thus result in a smaller spin canting of partially oxidized magnetite compared to the pristine stoichiometric magnetite²⁹.

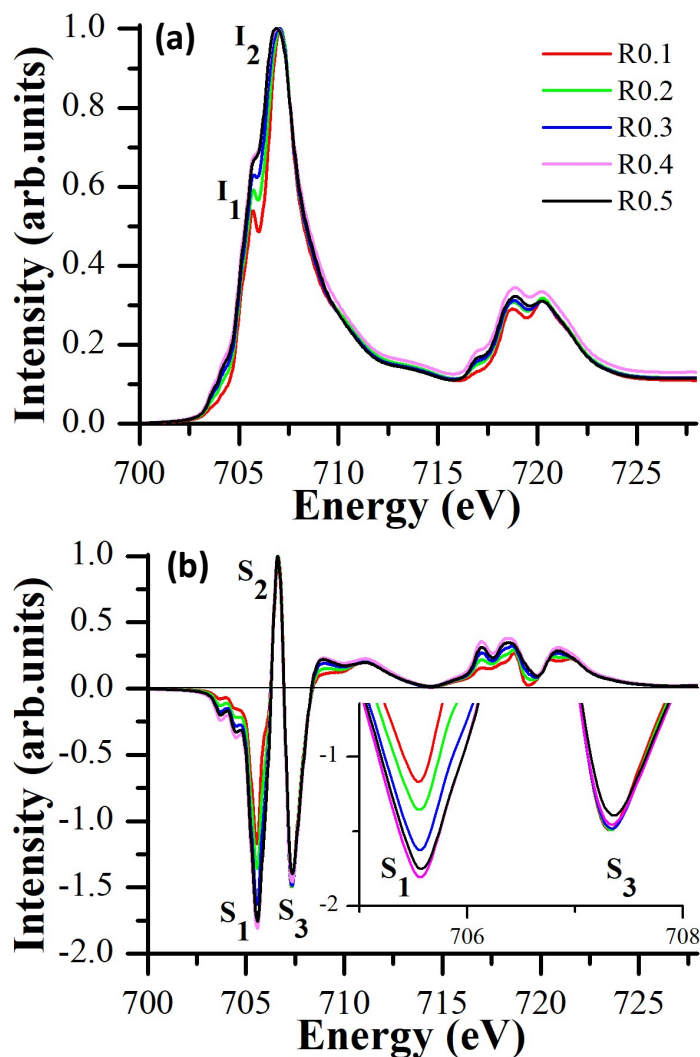


Figure 1. (a) Isotropic XAS and (b) normalized XMCD spectra of stoichiometric magnetite (R0.5) and its oxidation products (R0.1, R0.2, R0.3, and R0.4). XAS was normalized to the jump of edge and XMCD was normalized to the peak S_2 .

3.2 Impact of an oxidation-recharge cycle on the magnetite surface structure

Previous studies showed that partially oxidized magnetite can be converted into stoichiometric magnetite by dissolved Fe(II) amendment^{15–17}. Accordingly, a complete uptake of dissolved Fe(II) by R0.1 was observed when appropriate amounts of Fe(II) were added to reach $R_{\text{eff}} = 0.2, 0.3, 0.4,$ and 0.5 , at $\text{pH} = 8.5$. XRD and XAS analyses revealed, that the cell parameter and I_1/I_2 ratio of the magnetite with $R_{\text{eff}} = 0.5$ produced by the addition of Fe(II) to R0.1 was

1
2
3 similar to that of the pristine stoichiometric magnetite (Table S1, Figures S2 and S4), and TEM
4 evidenced no significant size or morphological evolution of the nanoparticles upon recharge
5 (Figure S1). The XMCD spectra of samples obtained by the recharge of R0.1 were very similar
6 to those obtained for the corresponding magnetites produced by oxidation of R0.5 (Figure 2).
7 However, the S_1 and S_3 peak intensities in the XMCD spectrum of the recharged R0.1 to R0.5
8 are larger than those of stoichiometric magnetite (R0.5). This might be attributed to decreased
9 spin canting after the oxidation-recharge cycle. Indeed, two mechanisms could explain the
10 recharge of partially oxidized magnetite into stoichiometric magnetite. Firstly, Mössbauer
11 spectroscopy investigations showed that adsorption of Fe(II) is followed by an electron transfer,
12 leading to the reduction of the octahedral Fe^{3+} atoms in the underlying magnetite to octahedral
13 Fe^{2+} atoms¹⁵. Secondly, isotopic exchange experiments suggested a fast Fe atom exchange
14 between magnetite and the aqueous solution²⁰. Both Fe^{2+} cations diffusing into the solid phase
15 and/or the redistribution of electron equivalents between the aqueous solution and the interior of
16 magnetite may involve recrystallization, as previously shown^{50–53}. This scenario is supported by
17 the Bragg peaks enlargement observed on XRD patterns (Figure S2). The determined apparent
18 crystallite size by Rietveld refinements, whose determination is affected by crystallographic
19 defects or internal strains for nanoparticles⁴⁸, increases from 6.3 nm to 9 nm after recharging
20 R0.1 up to $R = 0.5$. In fact, because the size of the particles hardly changes during the
21 oxidation/recharge process (9.6 ± 2.3 nm for R0.1, 11.3 ± 2.0 nm for the recharged sample;
22 Figure S1; Table S1), narrower peaks (and apparently larger crystallite size) after the recharge
23 process indicate a higher crystallinity compared to the initial material. Because surface spin
24 canting affects the XMCD signal of poorly-crystalline magnetite nanoparticles^{34,54}, our data
25 suggest that the recrystallization processes induced by the oxidation-recharge cycle lead to
26 decreased spin canting *i.e.* decreased structural disorder.
27
28
29
30
31
32
33
34
35
36
37
38
39
40
41
42
43
44
45
46
47
48
49
50
51
52
53
54
55
56
57
58
59
60

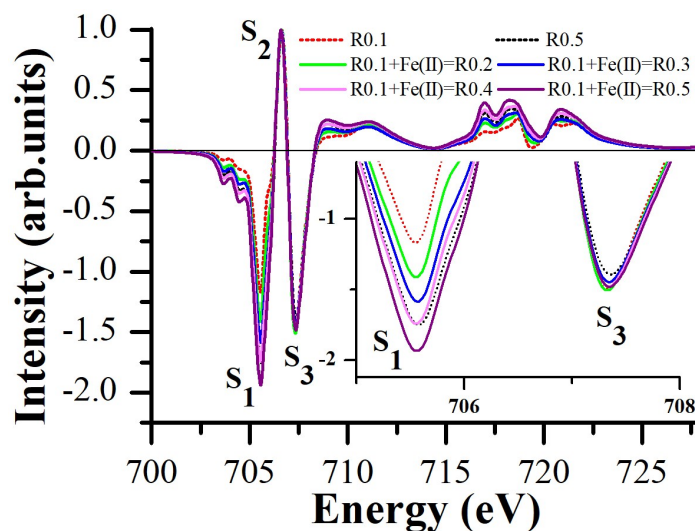


Figure 2. Normalized XMCD spectra of non-stoichiometric magnetite (R0.1) amended with dissolved Fe^{2+} to increase R_{eff} . Data are compared with pristine stoichiometric magnetite (R0.5).

3.3 Effects of Fe^{2+} excess on magnetite surface properties

Fe atom exchange and redistribution of electron equivalents between the aqueous solution and the interior of magnetite may not only occur during the recharge of partially oxidized magnetite but also the reaction of pristine stoichiometric magnetite with an excess of aqueous $\text{Fe}(\text{II})$ ^{20,21}. Therefore, “overloading” stoichiometric magnetite with dissolved $\text{Fe}(\text{II})$ may also affect the surface atomic ordering and related spin canting. To test this hypothesis, R0.5 was reacted with 250-2500 μM $\text{Fe}(\text{II})$ at pH 8.5. Complete uptake of $\text{Fe}(\text{II})$ by R0.5 was observed by spectrophotometric analysis, which leads to an apparent increase of R_{eff} with increasing added $[\text{Fe}(\text{II})]_{\text{aq}}$ (Table S1). Accordingly, XAS spectra exhibited an increase in I_1 compared to that of R0.5 (Figure 3a). This peak became predominant for $[\text{Fe}(\text{II})] = 2500 \mu\text{M}$ (Figure 3a), where the solid phase exhibits an $R_{\text{eff}} = 0.93$. Such a very intense I_1 peak suggests precipitation of a $\text{Fe}(\text{II})$ -solid phase. In the normalized XMCD spectra (Figure 3b), both the intensity of S_1 and S_3 increased with an increasing amount of added $\text{Fe}(\text{II})$ up to 1000 μM . Thus, spin canting effects decreased, allowing an increase of the magnetic properties. However, a large excess of $\text{Fe}(\text{II})$ (2500 μM) did not further affect the normalized XMCD signal, which confirms the formation of magnetically silent $\text{Fe}(\text{II})$ -solid phase at the magnetite surface. A comparable process was observed during the synthesis of titanomagnetites nanoparticles at large $\text{Fe}(\text{II})$ concentrations,

when Fe(II) could not enter the titanomagnetite structure.³⁰ We suspect that, given our experimental conditions, that Fe(II) oxide or hydroxide formed. The cell parameter determined by XRD analysis did not significantly differ between the overloaded magnetite (2500 μM) and the pristine R0.5 (Table S1), probably because of the amorphous structure of the Fe(II)-containing layer. TEM confirmed the formation of an amorphous layer at the magnetite surface (Figure S1). The presence of this Fe(II)-containing precipitate onto the magnetite surface explains the strong increase of I_1 , while the normalized XMCD spectrum remained unchanged (Figure 3b).

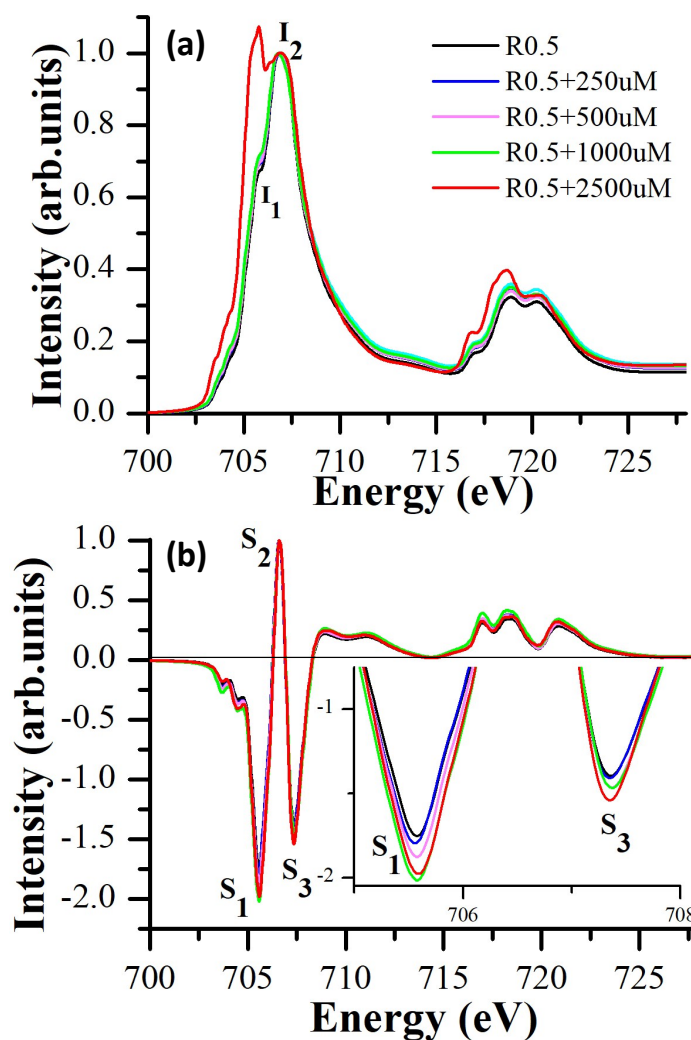


Figure 3. (a) Isotropic XAS and (b) normalized XMCD spectra of stoichiometric magnetite reacted with an excess of dissolved Fe²⁺ (250-2500 μM).

3.4 Determination of nanomagnetite stoichiometry using XMCD

The determination of the magnetite stoichiometry - or the mole fraction (X) of magnetite in the magnetite(Fe₃O₄)/maghemite(Fe_{8/3}O₄) solid solution - by XMCD is often based on linear combination fits (LCF) involving maghemite and stoichiometric magnetite references:

$$\text{Int}(\text{Sample}) = X \times \text{Int}(\text{Magnetite}) + (1-X) \times \text{Int}(\text{Maghemite}) \quad (3)$$

where “Int” is the XMCD signal intensity of the sample or a reference at a given energy, and the relationship between X and R_{eff} being given by the following equation where “n” refers to quantities of matter (moles):

$$X = n(\text{Fe}_3\text{O}_4) / (n(\text{Fe}_3\text{O}_4) + n(\text{Fe}_{8/3}\text{O}_4)) = 8R_{\text{eff}} / (3 + 2R_{\text{eff}}) \quad (4)$$

However, the present results show that the XMCD signal of nanomagnetite does not only depend on its stoichiometry but it can also be affected by the crystallinity at the nanoparticle surface and related spin canting effects. Hence, the XMCD signal depends on the alternation of redox conditions, because oxidation and reaction with Fe(II) lead to recrystallization at the nanoparticle surface. This may hamper the determination of magnetite stoichiometry by XMCD.

Given the size (around 10 nm) of the presently studied Fe_{3-δ}O₄ nanoparticles, the TEY used as surface detection mode, is also sensitive to the core of the nanoparticles. By making the approximation that the TEY probes the entire particle, although more sensitive to the surface, it is possible to use experimental values of R_{eff} measured by spectrophotometry (eq. 2) to estimate the respective XMCD signals of magnetite and maghemite by a least-square fit. Normalized XMCD spectra and R_{eff} of the four non-stoichiometric magnetites produced by oxidation of R0.5 were used for this purpose. The calculated spectrum of maghemite (R0) is qualitatively consistent with literature data^{27,28,49} and the intensity of peak S₃ is similar to that of the calculated spectrum of magnetite (R0.5), as expected in the absence of spin canting effects (Figure 4). Interestingly, if the XMCD spectrum of the pristine stoichiometric magnetite R0.5 is affected by spin canting, the oxidation-recharge cycle or the overloading with 1000 μM Fe(II) improved the XMCD signal and lead to similar spectra as the calculated one (Figure 4). This comparison suggests that this spectrum corresponds to the spin canting-free stoichiometric magnetite nanoparticles (~10nm), and then can be used as a good reference to determine magnetite stoichiometry by LCF of XMCD data.

1
2
3
4
5
6
7
8
9
10
11
12
13
14
15
16
17
18
19
20
21
22
23
24
25
26
27
28
29
30
31
32
33
34
35
36
37
38
39
40
41
42
43
44
45
46
47
48
49
50
51
52
53
54
55
56
57
58
59
60

Conversely, when neglecting spin canting effects, attempts to re-evaluate R_{eff} of the stoichiometric magnetite subjected to a complete oxidation-recharge cycle using the XMCD spectrum of the pristine stoichiometric magnetite, can be made with equations 3-4 and a least-square fit, in which the maghemite term is set to 0. The fitted spectrum over the energy range 700-715eV (Figure 4b) accurately predicts the intensity of the $\text{Fe(II)}_{\text{Oh}}$ peak while only slightly overestimating that of the $\text{Fe(III)}_{\text{Oh}}$ and $\text{Fe(III)}_{\text{Td}}$ peaks, respectively, hence providing a reasonable estimate for the present purpose. The corresponding value of R_{eff} equals 0.57. Repeating the same exercise for the overloaded stoichiometric magnetite with 1000 μM Fe(II) leads to $R_{\text{eff}} = 0.61$ (not shown). These larger values than 0.5 might suggest the formation of hyperstoichiometric or “cation-excess” magnetite, as previously suggested.²¹ Therefore, although the presently observed spin canting effect is relatively small, this demonstrates that its omission has important consequence for the determination of the magnetite stoichiometry.

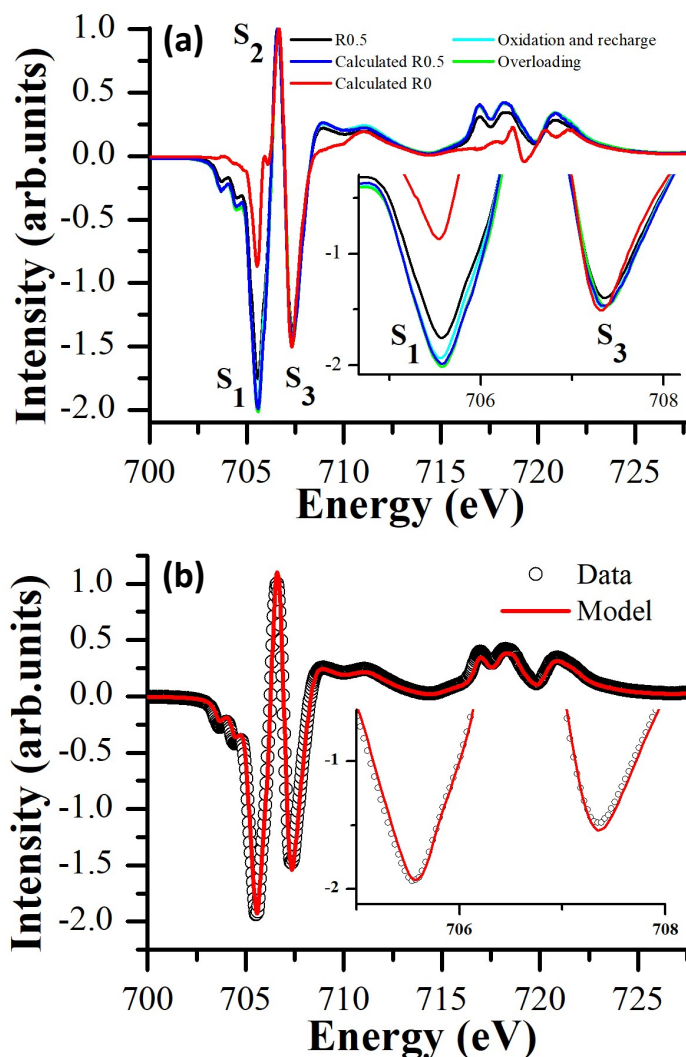


Figure 4. (a) Normalized XMCD spectra of pristine stoichiometric magnetite (R0.5), amended R0.1 with Fe(II) (“oxidation and recharge”), amended R0.5 with 1000 μ M Fe(II) (“overloading”), and comparison with the calculated spectra of maghemite and stoichiometric magnetite (“calculated” R0 and R0.5, respectively). (b) Normalized XMCD spectrum of the stoichiometric magnetite subjected to a complete oxidation-recharge cycle (data) fitted using equations 3-4 and the XMCD spectrum of the pristine stoichiometric magnetite (model).

Another approach can be used to estimate magnetite stoichiometry. An indicator (S) was defined in order to follow the evolution of peak intensities versus stoichiometry³⁴:

$$S = (S_1 + S_2) / (S_2 + S_3) \quad (5)$$

This approach can also be used to compare our results with literature data. The value of S is plotted against X determined by acid digestion in Figure 5 for $X \leq 1$ (other data are given in Table S1). An error of 5% is assumed on the determination of S. Measured values²⁸ or presently estimated ones for maghemite ($X = 0$) agree relatively well ($S = 0.69$ and 0.75 , respectively). The presently synthesized pristine stoichiometric magnetite exhibits S approximately equal to 1.15, in excellent agreement with about 10 nm stoichiometric magnetite particles synthesized by coprecipitation²¹ or with few nanometer thin films²⁸. Spectra recorded after an oxidation-recharge cycle, in the presence of excess Fe(II) and the calculated spectrum of R0.5 lead to $S = 1.22$, in agreement with the experimental study²¹ which contained stoichiometric magnetite with $1000\mu\text{M}$ Fe(II) ($S = 1.25$). The following relationship was graphically found to estimate X (± 0.05 X units) from the S value:

$$X = (S - 0.737) / 0.446 \quad (6)$$

However, it appears that very different XMCD spectra were published for stoichiometric magnetite, leading to a broad range of S values, from 1.15 to 1.46 (Table S2)^{21,24-29}. Such a large variation cannot be attributed to a variable Fe(II) content between the studied magnetites. Instead, we suspect that the synthesis procedures can affect the morphology and surface characteristics of stoichiometric magnetite^{55,56}. For instance, biogenic magnetite nanoparticles (20-30 nm) are more crystalline than abiotic ones^{24,25}, and produce larger S values (1.30), while magnetite nanoparticles synthesized by thermal decomposition (5-22 nm) are also well crystallized with large S values^{27,49} (Table S2). Therefore, the determined reference stoichiometric magnetite XMCD spectrum (eq. 3) and the present calibration using X versus S (eq. 6) might be only used to determine the stoichiometry of about 10 nm-sized precipitated particles. Further studies are required to quantify the combined effects of magnetite stoichiometry, particle size, and crystallinity on the XMCD spectra.

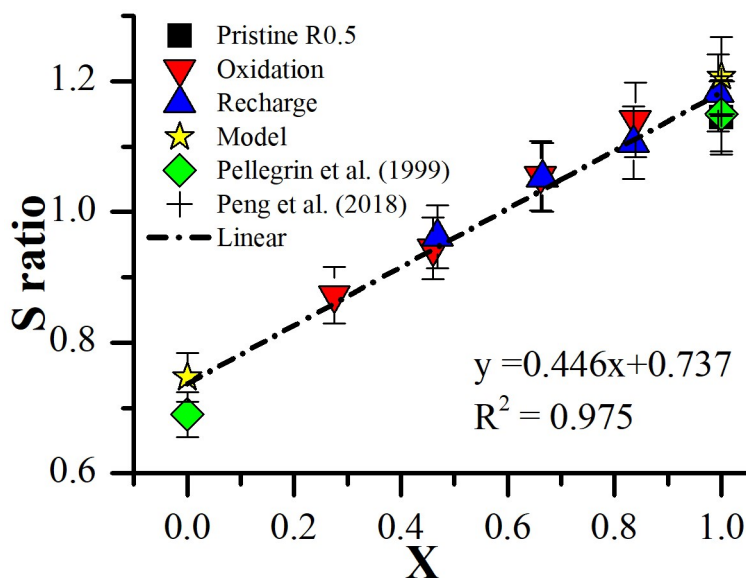


Figure 5. S ratio (eq. 5) versus the mole fraction of magnetite (X) for all samples presently analyzed by XMCD. S values are compared with that obtained from previous studies^{21,28} and presently calculated spectra of R0 and R0.5 (eq. 3).

4. Conclusions

Magnetite nanoparticles have broad implications in geochemistry, environmental science, and materials science, due to their large reactivity, good inherent magnetism, and redox properties. Although the surface reactivity of $\text{Fe}_{3-\delta}\text{O}_4$ nanoparticles is extensively investigated, knowledge regarding the transformation of magnetite into maghemite, and *vice versa*, is limited. In the present study, magnetite stoichiometry was tuned in aqueous suspension by adding appropriate amounts of H_2O_2 or dissolved Fe^{2+} . The experimental dataset presented in this work confirmed that XMCD analysis may be used to follow the Fe(II)/Fe(III) ratio^{21,24,28,30} but caution with respect to spin canting or the degree of structural order of the minerals is required.^{29,33} Indeed, oxidation as well as Fe^{2+} diffusion into the solid phase and/or redistribution of electron equivalents between the aqueous solution and the magnetite bulk implied surface recrystallization processes, thereby affecting XMCD signals. This was evidenced through an oxidation-recharge cycle of the pristine magnetite and by adding an excess of dissolved Fe(II) to a stoichiometric magnetite suspension.

The implication of the present work is twofold. First, it provides a more comprehensive examination of the dynamic behavior of the magnetite-maghemite system in aqueous solutions. Second, these results uncover a more accurate method for the determination of the stoichiometry of nanosized magnetite particles (~ 10 nm) by XMCD. Therefore, for future studies, the present results might be useful to further elucidate, for instance, the impact of magnetite stoichiometry on the redox transformation of various organic and inorganic pollutants or the role of microorganisms for magnetite stoichiometry.

CRedit authorship contribution statement

Phoomipat Jungcharoen: Writing -original draft, Data curation, Investigation, Visualization. **Mathieu Pédrot:** Writing - review & editing, Resources, Supervision, Project administration, Funding acquisition. **Fadi Choueikani:** Investigation, Data curation, Writing - review & editing. **Mathieu Pasturel:** Investigation, Data curation, Writing - review & editing. **Khalil Hanna:** Writing - review & editing. **Frank Heberling:** Writing - review & editing. **Marawit Tesfa:** Investigation, Data curation, Writing - review & editing. **Rémi Marsac:** Writing - review & editing, Resources, Supervision, Project administration, Funding acquisition.

Acknowledgments

This work was supported by Campus France, Khon Kaen University (Thailand), the C-FACTOR project funded by ANR (project number ANR-18-CE01-0008), the SURFNANO project funded by the CNRS-INSU EC2CO program, and the SynFeSol project funded by the Brittany Region (AAP TRANSFERT 2019). Through the support of the GeOHeLiS analytical platform of Rennes University, this publication is also supported by the European Union through the European Regional Development Fund (FEDER), the French Ministry of Higher Education and Research, the French Region of Brittany and Rennes Metropole. The authors acknowledge the SOLEIL synchrotron for beamtime allocation at the DEIMOS beamline (proposal 20200250). The authors are grateful to V. Dorcet and L. Rault for the assistance in TEM experiments performed on the THEMIS platform (ScanMAT, UMS 2011 University of Rennes 1-CNRS; CPER-FEDER 2007–2014).

References

- 1 M. Usman, J. M. Byrne, A. Chaudhary, S. Orsetti, K. Hanna, C. Ruby, A. Kappler and S. B. Haderlein, Magnetite and Green Rust: Synthesis, Properties, and Environmental Applications of Mixed-Valent Iron Minerals, *Chem. Rev.*, 2018, **118**, 3251–3304.
- 2 R. Weissleder, M. Nahrendorf and M. J. Pittet, Imaging macrophages with nanoparticles, *Nature Mater*, 2014, **13**, 125–138.
- 3 C. Li, A targeted approach to cancer imaging and therapy, *Nature Mater*, 2014, **13**, 110–115.
- 4 S. Zanganeh, G. Hutter, R. Spitler, O. Lenkov, M. Mahmoudi, A. Shaw, J. S. Pajarinen, H. Nejadnik, S. Goodman, M. Moseley, L. M. Coussens and H. E. Daldrup-Link, Iron oxide nanoparticles inhibit tumour growth by inducing pro-inflammatory macrophage polarization in tumour tissues, *Nature Nanotech*, 2016, **11**, 986–994.
- 5 D. Wang, R. Kou, D. Choi, Z. Yang, Z. Nie, J. Li, L. V. Saraf, D. Hu, J. Zhang, G. L. Graff, J. Liu, M. A. Pope and I. A. Aksay, Ternary Self-Assembly of Ordered Metal Oxide–Graphene Nanocomposites for Electrochemical Energy Storage, *ACS Nano*, 2010, **4**, 1587–1595.
- 6 X. Zhu, Y. Zhu, S. Murali, M. D. Stoller and R. S. Ruoff, Nanostructured Reduced Graphene Oxide/Fe₂O₃ Composite As a High-Performance Anode Material for Lithium Ion Batteries, *ACS Nano*, 2011, **5**, 3333–3338.
- 7 L. M. Rossi, N. J. S. Costa, F. P. Silva and R. Wojcieszak, Magnetic nanomaterials in catalysis: advanced catalysts for magnetic separation and beyond, *Green Chem.*, 2014, **16**, 2906.
- 8 P. V. Nidheesh, Heterogeneous Fenton catalysts for the abatement of organic pollutants from aqueous solution: a review, *RSC Adv.*, 2015, **5**, 40552–40577.
- 9 P. Xu, G. M. Zeng, D. L. Huang, C. L. Feng, S. Hu, M. H. Zhao, C. Lai, Z. Wei, C. Huang, G. X. Xie and Z. F. Liu, Use of iron oxide nanomaterials in wastewater treatment: A review, *Science of The Total Environment*, 2012, **424**, 1–10.
- 10 J. Deng, S. Bae, S. Yoon, M. Pasturel, R. Marsac and K. Hanna, Adsorption capacity of the corrosion products of nanoscale zerovalent iron for emerging contaminants, *Environ. Sci.: Nano*, 2020, **7**, 3773–3782.
- 11 R. M. Cornell and U. Schwertmann, *Also of interest Iron Oxides in the Laboratory*, 2003.
- 12 I. A. M. Ahmed and B. A. Maher, Identification and paleoclimatic significance of magnetite nanoparticles in soils, *Proc Natl Acad Sci USA*, 2018, **115**, 1736–1741.
- 13 P. C. Lippert, Big discovery for biogenic magnetite, *PNAS*, 2008, **105**, 17595–17596.
- 14 J. M. Byrne, N. Klueglein, C. Pearce, K. M. Rosso, E. Appel and A. Kappler, Redox cycling of Fe(II) and Fe(III) in magnetite by Fe-metabolizing bacteria, *Science*, 2015, **347**, 1473–1476.
- 15 C. A. Gorski and M. M. Scherer, Influence of Magnetite Stoichiometry on Fe^{II} Uptake and Nitrobenzene Reduction, *Environ. Sci. Technol.*, 2009, **43**, 3675–3680.
- 16 C. A. Gorski, J. T. Nurmi, P. G. Tratnyek, T. B. Hofstetter and M. M. Scherer, Redox Behavior of Magnetite: Implications for Contaminant Reduction, *Environ. Sci. Technol.*, 2010, **44**, 55–60.
- 17 W. Cheng, R. Marsac and K. Hanna, Influence of Magnetite Stoichiometry on the Binding of Emerging Organic Contaminants, *Environ. Sci. Technol.*, 2018, **52**, 467–473.
- 18 D. E. Latta, C. A. Gorski, M. I. Boyanov, E. J. O’Loughlin, K. M. Kemner and M. M. Scherer, Influence of Magnetite Stoichiometry on UVI Reduction, *Environ. Sci. Technol.*, 2012, **46**, 778–786.
- 19 I. A. M. Ahmed and B. A. Maher, Identification and paleoclimatic significance of magnetite nanoparticles in soils, *PNAS*, 2018, **115**, 1736–1741.
- 20 C. A. Gorski, R. M. Handler, B. L. Beard, T. Pasakarnis, C. M. Johnson and M. M. Scherer, Fe Atom Exchange between Aqueous Fe²⁺ and Magnetite, *Environ. Sci. Technol.*, 2012, **46**, 12399–12407.
- 21 H. Peng, C. I. Pearce, W. Huang, Z. Zhu, A. T. N’Diaye, K. M. Rosso and J. Liu, Reversible Fe(II) uptake/release by magnetite nanoparticles, *Environ. Sci.: Nano*, 2018, **5**, 1545–1555.

- 22 R. Marsac, M. Pasturel and K. Hanna, Reduction Kinetics of Nitroaromatic Compounds by Titanium-Substituted Magnetite, *J. Phys. Chem. C*, 2017, **121**, 11399–11406.
- 23 G. van der Laan and A. I. Figueroa, X-ray magnetic circular dichroism—A versatile tool to study magnetism, *Coordination Chemistry Reviews*, 2014, **277–278**, 95–129.
- 24 C. Carvallo, P. Saintavit, M.-A. Arrio, N. Menguy, Y. Wang, G. Ona-Nguema and S. Brice-Profeta, Biogenic vs. abiogenic magnetite nanoparticles: A XMCD study, *American Mineralogist*, 2008, **93**, 880–885.
- 25 V. S. Coker, C. I. Pearce, R. A. D. Pattrick, G. van der Laan, N. D. Telling, J. M. Charnock, E. Arenholz and J. R. Lloyd, Probing the site occupancies of Co-, Ni-, and Mn-substituted biogenic magnetite using XAS and XMCD, *American Mineralogist*, 2008, **93**, 1119–1132.
- 26 F. Jiménez-Villacorta, C. Prieto, Y. Huttel, N. D. Telling and G. van der Laan, X-ray magnetic circular dichroism study of the blocking process in nanostructured iron-iron oxide core-shell systems, *Phys. Rev. B*, 2011, **84**, 172404.
- 27 A. Kuzmin and J. Chaboy, EXAFS and XANES analysis of oxides at the nanoscale, *IUCrJ*, 2014, **1**, 571–589.
- 28 E. Pellegrin, M. Hagelstein, S. Doyle, H. O. Moser, J. Fuchs, D. Vollath, S. Schuppler, M. A. James, S. S. Saxena, L. Niesen, O. Rogojuanu, G. A. Sawatzky, C. Ferrero, M. Borowski, O. Tjernberg and N. B. Brookes, Characterization of Nanocrystalline g-Fe₂O₃ with Synchrotron Radiation Techniques, 1999, **215**, 797–801.
- 29 L. Signorini, L. Pasquini, F. Boscherini, E. Bonetti, I. Letard, S. Brice-Profeta and P. Saintavit, Local magnetism in granular iron/iron oxide nanostructures by phase- and site-selective x-ray magnetic circular dichroism, *Phys. Rev. B*, 2006, **74**, 014426.
- 30 C. I. Pearce, O. Qafoku, J. Liu, E. Arenholz, S. M. Heald, R. K. Kukkadapu, C. A. Gorski, C. M. B. Henderson and K. M. Rosso, Synthesis and properties of titanomagnetite (Fe_{3-x}Ti_xO₄) nanoparticles: A tunable solid-state Fe(II/III) redox system, *Journal of Colloid and Interface Science*, 2012, **387**, 24–38.
- 31 K. A. Stoerzinger, C. I. Pearce, T. C. Droubay, V. Shutthanandan, Z. Liu, E. Arenholz and K. M. Rosso, Structure, Magnetism, and the Interaction of Water with Ti-Doped Fe₃O₄ Surfaces, *Langmuir*, 2019, **35**, 13872–13879.
- 32 M. Darbandi, F. Stromberg, J. Landers, N. Reckers, B. Sanyal, W. Keune and H. Wende, Nanoscale size effect on surface spin canting in iron oxide nanoparticles synthesized by the microemulsion method, *J. Phys. D: Appl. Phys.*, 2012, **45**, 195001.
- 33 C. Graf, C. Goroncy, P. Stumpf, E. Weschke, C. Boeglin, H. Ronneburg and E. Rühl, Local Magnetic and Electronic Structure of the Surface Region of Postsynthesis Oxidized Iron Oxide Nanoparticles for Magnetic Resonance Imaging, *J. Phys. Chem. C*, 2015, **119**, 19404–19414.
- 34 S. Brice-Profeta, M.-A. Arrio, E. Tronc, N. Menguy, I. Letard, C. Cartier dit Moulin, M. Noguès, C. Chanéac, J.-P. Jolivet and Ph. Saintavit, Magnetic order in - nanoparticles: a XMCD study, *Journal of Magnetism and Magnetic Materials*, 2005, **288**, 354–365.
- 35 R. Massart, Preparation of aqueous magnetic liquids in alkaline and acidic media, *IEEE Transactions on Magnetics*, 1981, **17**, 1247–1248.
- 36 E. Demangeat, M. Pédrot, A. Dia, M. Bouhnik-le-Coz, F. Grasset, K. Hanna, M. Kamagate and F. Cabello-Hurtado, Colloidal and chemical stabilities of iron oxide nanoparticles in aqueous solutions: the interplay of structural, chemical and environmental drivers, *Environ. Sci.: Nano*, 2018, **5**, 992–1001.
- 37 R. Marsac, M. Pasturel and K. Hanna, Reduction Kinetics of Nitroaromatic Compounds by Titanium-Substituted Magnetite, *J. Phys. Chem. C*, 2017, **121**, 11399–11406.

- 1
2
3
4
5
6
7
8
9
10
11
12
13
14
15
16
17
18
19
20
21
22
23
24
25
26
27
28
29
30
31
32
33
34
35
36
37
38
39
40
41
42
43
44
45
46
47
48
49
50
51
52
53
54
55
56
57
58
59
60
- 38 C. A. Gorski and M. M. Scherer, Determination of nanoparticulate magnetite stoichiometry by Mossbauer spectroscopy, acidic dissolution, and powder X-ray diffraction: A critical review, *American Mineralogist*, 2010, **95**, 1017–1026.
- 39 W. B. Fortune and M. G. Mellon, Determination of Iron with o-Phenanthroline: A Spectrophotometric Study, *Ind. Eng. Chem. Anal. Ed.*, 1938, **10**, 60–64.
- 40 P. Ohresser, E. Otero, F. Choueikani, K. Chen, S. Stanescu, F. Deschamps, T. Moreno, F. Polack, B. Lagarde, J.-P. Daguere, F. Marteau, F. Scheurer, L. Joly, J.-P. Kappler, B. Muller, O. Bunau and Ph. Saintavit, DEIMOS: A beamline dedicated to dichroism measurements in the 350–2500 eV energy range, *Review of Scientific Instruments*, 2014, **85**, 013106.
- 41 J. Rodríguez-Carvajal, Recent advances in magnetic structure determination by neutron powder diffraction, *Physica B: Condensed Matter*, 1993, **192**, 55–69.
- 42 J. Rodríguez-Carvajal and T. Roisnel, Line Broadening Analysis Using FullProf*, <https://www.scientific.net/MSF.443-444.123>, (accessed 19 February 2021).
- 43 P. Ohresser, E. Otero, F. Choueikani, K. Chen, S. Stanescu, F. Deschamps, T. Moreno, F. Polack, B. Lagarde, J.-P. Daguere, F. Marteau, F. Scheurer, L. Joly, J.-P. Kappler, B. Muller, O. Bunau and Ph. Saintavit, DEIMOS: A beamline dedicated to dichroism measurements in the 350–2500 eV energy range, *Review of Scientific Instruments*, 2014, **85**, 013106.
- 44 N. Daffé, F. Choueikani, S. Neveu, M.-A. Arrio, A. Juhin, P. Ohresser, V. Dupuis and P. Saintavit, Magnetic anisotropies and cationic distribution in CoFe₂O₄ nanoparticles prepared by co-precipitation route: Influence of particle size and stoichiometry, *Journal of Magnetism and Magnetic Materials*, 2018, **460**, 243–252.
- 45 K. Sartori, G. Cotin, C. Bouillet, V. Halté, S. Bégin-Colin, F. Choueikani and B. P. Pichon, Strong interfacial coupling through exchange interactions in soft/hard core–shell nanoparticles as a function of cationic distribution, *Nanoscale*, 2019, **11**, 12946–12958.
- 46 M. Gotić, G. Koščec and S. Musić, Study of the reduction and reoxidation of substoichiometric magnetite, *Journal of Molecular Structure*, 2009, **924–926**, 347–354.
- 47 J. B. Yang, X. D. Zhou, W. B. Yelon, W. J. James, Q. Cai, K. V. Gopalakrishnan, S. K. Malik, X. C. Sun and D. E. Nikles, Magnetic and structural studies of the Verwey transition in Fe₃–δO₄ nanoparticles, *Journal of Applied Physics*, 2004, **95**, 7540–7542.
- 48 D. Balzar, N. Audebrand, M. R. Daymond, A. Fitch, A. Hewat, J. I. Langford, A. Le Bail, D. Louër, O. Masson, C. N. McCowan, N. C. Popa, P. W. Stephens and B. H. Toby, Size–strain line-broadening analysis of the ceria round-robin sample, *J Appl Cryst*, 2004, **37**, 911–924.
- 49 J. Park, K. An, Y. Hwang, J.-G. Park, H.-J. Noh, J.-Y. Kim, J.-H. Park, N.-M. Hwang and T. Hyeon, Ultra-large-scale syntheses of monodisperse nanocrystals, *Nature Mater*, 2004, **3**, 891–895.
- 50 C. M. Hansel, S. G. Benner and S. Fendorf, Competing Fe(II)-Induced Mineralization Pathways of Ferrihydrite, *Environ. Sci. Technol.*, 2005, **39**, 7147–7153.
- 51 R. M. Handler, B. L. Beard, C. M. Johnson and M. M. Scherer, Atom Exchange between Aqueous Fe(II) and Goethite: An Fe Isotope Tracer Study, *Environ. Sci. Technol.*, 2009, **43**, 1102–1107.
- 52 A. M. Jones, R. N. Collins, J. Rose and T. D. Waite, The effect of silica and natural organic matter on the Fe(II)-catalysed transformation and reactivity of Fe(III) minerals, *Geochimica et Cosmochimica Acta*, 2009, **73**, 4409–4422.
- 53 L. Yang, C. I. Steefel, M. A. Marcus and J. R. Bargar, Kinetics of Fe(II)-Catalyzed Transformation of 6-line Ferrihydrite under Anaerobic Flow Conditions, *Environ. Sci. Technol.*, 2010, **44**, 5469–5475.
- 54 M. Darbandi, F. Stromberg, J. Landers, N. Reckers, B. Sanyal, W. Keune and H. Wende, Nanoscale size effect on surface spin canting in iron oxide nanoparticles synthesized by the microemulsion method, *J. Phys. D: Appl. Phys.*, 2012, **45**, 195001.
- 55 C. Ravikumar and R. Bandyopadhyaya, Mechanistic Study on Magnetite Nanoparticle Formation by Thermal Decomposition and Coprecipitation Routes, *J. Phys. Chem. C*, 2011, **115**, 1380–1387.

1
2
3 56 M. Unni, A. M. Uhl, S. Savliwala, B. H. Savitzky, R. Dhavalikar, N. Garraud, D. P. Arnold, L. F.
4 Kourkoutis, J. S. Andrew and C. Rinaldi, Thermal Decomposition Synthesis of Iron Oxide Nanoparticles
5 with Diminished Magnetic Dead Layer by Controlled Addition of Oxygen, *ACS Nano*, 2017, **11**, 2284–
6 2303.
7